Received: 5 August 2024 | Revised: 28 September 2024 | Accepted: 24 October 2024

DOI: 10.1002/pc.29247

RESEARCH ARTICLE

Polymer COMPOSITES WILEY

Tribologically enhanced self-healing hybrid laminates for wind turbine applications

Kemal Hasirci[1] | **Berkay Ergene**[2] | **Alaeddin Burak Irez**[1,3]

[1]Department of Mechanical Engineering, Faculty of Mechanical Engineering, Istanbul Technical University (ITU), Istanbul, Türkiye

[2]Department of Mechanical Engineering, Faculty of Technology, Pamukkale University, Denizli, Türkiye

[3]Department of Biomedical Engineering, Carnegie Mellon University, Pittsburgh, Pennsylvania, USA

Correspondence
Alaeddin Burak Irez, Department of Mechanical Engineering, Faculty of Mechanical Engineering, Istanbul Technical University (ITU), Istanbul 34437, Türkiye.
Email: irez@itu.edu.tr

Funding information
Bilimsel Araştırma Projeleri Birimi, İstanbul Teknik Üniversitesi, Grant/Award Number: MGA-2022-43400

Abstract

Wind turbines are subjected to extreme weather and load conditions; hence, high strength and impact resistance are required. Furthermore, wind turbine blades can be subjected to impact loads such as bird strikes, resulting in the formation of microcracks. Self-healing capsules can be used to mend turbine blades for microscale damage. The incorporation of self-healing capsules may cause a decrease in the mechanical characteristics of the composites prior to impact resistance, which can be compensated for with efficient fillers such as silicon carbide whiskers (SiC_w). Thus, a novel hybrid composite structure is examined with the advantage of using a self-healing mechanism and SiC_w reinforcement. Tensile, tribological, and Charpy impact tests were performed to characterize the mechanical and tribological properties, which were supported with microscopic observations. Multiple experimental characterizations were performed to investigate the impact, and the ultimate tensile strength (UTS) and energy absorption capacity of the structure were shown to increase by 32% and 45%, respectively, with the addition of SiC_w. The presence of self-healing agents provides a 5% rise in UTS after enough time for healing following the collision. The structure's tribological performance is improved by 10% in wear resistance and 20% in friction coefficient.

Highlights

- Hybrid laminated composite structure with silicon carbide whisker and self-healing capsules.
- Tensile and Charpy impact tests conducted with microscopic observations
- Increased ultimate tensile strength and energy absorption capacity by 32% and 45%.
- Tribological improvement by 10% in wear resistance and 20% in friction coefficient.

KEYWORDS

bird strike, hybrid composites, self-healing, silicon carbide whiskers, wind turbines

1 | INTRODUCTION

Over the past few decades, wind power has emerged as a prominent source of renewable energy, mostly due to the establishment of onshore and offshore wind farms. Numerous studies are currently being conducted to enhance the efficiency and reduce the cost of wind turbines. Hybrid materials, namely hybrid laminate composites, are now under investigation for their potential application in wind turbine blades. In comparison to conventional blades, the utilization of hybrid composite material blades presents advantages in terms of improved strength, stiffness, efficiency, and cost-effectiveness.[1–4] Moreover, considering the increasing costs related to the maintenance of wind turbines, there is a growing trend to design turbine blades that exhibit resistance against wind erosion and bird strikes.[5,6] For this purpose, several developments have been realized in the composite structures.[7,8]

Bird strikes are an important consideration when analyzing wind turbine blade damage.[9–12] An estimated 20,000 incidents of bird strikes occur annually on wind turbines in the United States. These incidents culminate in an average of 4.27 bird fatalities per turbine.[13–16] As a result, bird strikes must be considered a significant criterion in the design process for wind turbines. Several studies have been conducted to design, model, and test the bird strike event for laminate composites with various failure modes that are simulated through material damage, stiffness reduction, and element removal, and these models were utilized to optimize the stacking sequence, which resulted in improved impact resistance capability.[17–19] Different composite materials exhibit different deformation behavior against projectile impact like bird impacts. The variability in this behavior is contingent upon the parameters related to strength and fracture energy.[20–22] Thus, the differentiation in the material properties can represent varying damage mechanisms. Four distinct types of damage may result from impact loading: delamination, matrix cracking, fiber breaking, and complete perforation. During low-velocity impacts,[23–27] the composite laminate undergoes a sequential pattern of damage as the amount of impact energy rises.

Materials, particularly composites, have incorporated self-healing mechanisms to repair microcracks and other forms of damage resulting from dynamic loading and impact during service. Cutting-edge aircraft components, such as engines, fuselages, and coatings, exhibit a diverse array of self-healing materials, methods, and applications. The healing mechanism may exhibit variability across various polymer matrices. Thermosets include the encapsulation of uncured resins, such as epoxy, within microcapsules. Subsequently, the capsules are incorporated into the resin and uniformly dispersed throughout the manufacturing procedure of the composite material. When this composite is used in a component and subjected to impacts, the capsules tear, causing the resin to fill the resulting cracks. The uncured resin undergoes solidification in the presence of inherent hardening agents inside the composite. By healing the cracks, the composite material can be effectively repaired and maintained for further usage.[28–34] In the research conducted by Hayes et al., a novel self-healing technology based on a solid-state thermoset repair system was employed in the structural composite. The findings of the study demonstrated that the composites exhibited a restoration of 50% to 70% of their initial failure strength following the healing process.[35] Furthermore, it was determined that a capsule content of 7.5 wt% exhibited the highest efficiency in terms of Charpy impact testing.[29] The fracture characteristics of a carbon fiber-reinforced polymer matrix composite that incorporated a microencapsulated healing agent were investigated in a separate study. Recently fractured specimens were bonded together using light pressure and allowed to heal at room temperature after 48 hours.[36] Following subsequent tests, the healing efficiency, as measured by the restoration of interlaminar fracture toughness, was found to be around 38% on average, with a maximum value of over 45%. An increase in healing temperature to 80 degrees Celsius resulted in an average improvement in healing efficiency of 66%, with a peak of 80%.[36]

Under typical circumstances, the wind turbine structure is resilient enough to endure impact damage caused by bird collisions. Nevertheless, in order to endure severe wind and rotor stop conditions, it is imperative that the material enhance its strength, wear resistance, friction coefficient, and fracture toughness. In addition to that, the wind turbine structure can be optimized as a hybrid structure, and the layup of each material can be determined in order to reduce the cost of the structure.[37,38] Various techniques, including fiber orientation alignment, matrix modification, heat treatment, and the use of fillers, can enhance the mechanical, damage, and tribological performance parameters.[39–43] The composite laminates are improved in terms of strength, wear resistance, friction coefficient, and fracture toughness by including efficient fillers. There are a variety of efficient fillers available in the market used by the researchers. Silicon carbide (SiC) and silicon nitride (Si_3N_4) are the most common ceramic whiskers with commercial significance. Other ceramic whiskers include: AlO whiskers, K_4TiO_4 whiskers, and aluminum borate (H_3AlBO_2) whiskers. SiC_w are often used in aluminum alloy matrix composites because of their favorable mechanical properties, density, and cost. They can be synthesized using carbothermal reduction or chemical vapor deposition (CVD). Whiskered ceramic inserts are used in the aerospace, automotive, and general machining industries to cut hard materials. They are reinforced with whiskers to increase their toughness,

hardness, and high-temperature resistance. However, SiC_w exhibits remarkable mechanical properties as a filler, such as a low bulk density, high strength, and resistance to deformation at high temperatures due to its covalent bonding.[44] Moreover, SiC_w has exceptional thermal, electrical, chemical, and nuclear characteristics, including elevated thermal conductivity, exceptional resistance to wear.[45–47] Furthermore, it has a notable level of resistance to oxidation and chemical substances.[48,49] Hence, the utilization of silicon carbide whiskers (SiC_w) holds promise in enhancing the mechanical and tribological characteristics of laminate composites to a considerable extent. Numerous studies have been undertaken to explore the application of SiC_w in composite materials using diverse methodologies. A study was conducted to examine the evolution of interlaminar fracture toughness by developing carbon fiber-epoxy composites that incorporated SiC_w into the epoxy matrix at different weight ratios ranging from 0 to 1.5 wt%. The fracture toughness of the composite material with 0.5 wt% SiC_w was found to be the highest, indicating that a whisker weight ratio of 0.5 wt% is the most favorable among the specimens that were examined.[50] The mechanical properties of high-performance polymer (PA6) composites were enhanced through the incorporation of one-dimensional SiC_w, as demonstrated in a separate investigation. By including 2 wt% SiC_w, the tensile strength of composites was increased by 37.6%, resulting in a value of 58.2 MPa. Moreover, the incorporation of 30% SCWS results in a decrease in the friction coefficient of the composite material from 0.31 to 0.15, hence demonstrating enhanced resistance to abrasion.[51] Therefore, it has been decided to consider a whisker weight ratio of 0.5 wt% in the laminated composite structure as detailed in Section 4.1.

Hence, the objective of this study is to contribute to the development of self-healing hybrid composites reinforced with SiC_w. Through this contribution, it is aimed to enhance the mechanical and tribological performance of the developed composites, resulting in reduced maintenance and operational costs.

The present study entails the fabrication of hybrid laminate composites, followed by the application of impact loading to induce damage to specific composite groups, and subsequently observing the resulting healing process. Furthermore, the impact of incorporating SiC_w on mechanical characteristics was assessed by the utilization of tensile and Charpy impact tests. Ultimately, the researchers conducted microscopic examinations utilizing optical microscopy techniques in order to ascertain the processes of damage and the spatial arrangement of the fillers.

Subsequently, tribological evaluations were carried out on the developed composites to investigate the influence of SiCw on both the wear resistance and friction coefficient of the laminate composites.

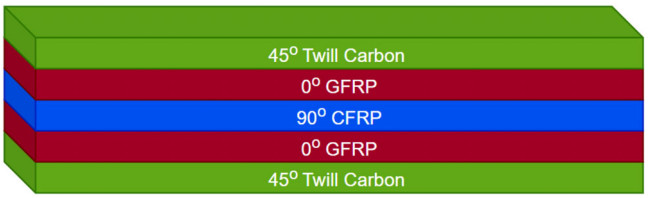

FIGURE 1 Stacking sequence of hybrid laminate composite.

2 | MATERIALS AND METHODS

This study involved the production of epoxy matrix composites reinforced with unidirectional (UD) glass fiber fabrics, UD carbon fiber fabrics, and twill woven carbon fabrics. L300 UD E-glass fiber fabrics (Metyx®), 200 GSM Twill Woven Carbon (Metyx), and DW 300 UD Carbon (DowAksa®) were used for the manufacture of laminated composites (see Figure S4). The laminate composites consist of five layers (45/0/90/0/45) (see Figure 1). To increase impact resistance, 45° twill carbon is employed as woven fabric composites demonstrate increased stiffness and strength when subjected to shear loading compared to UD composites, as long as the fiber-matrix combination and fiber volume ratio are consistent[52,53]; two layers of 0°GFRP and 1 layer of 90°CFRP are selected to have high strength in the 0° direction. The properties of laminates are given in Table 1.

Based on the results of stiffness calculations, it can be observed that the values of E1 (elastic modulus in the X direction) and E2 (elastic modulus in the Y direction) closely correspond to orthotropic structures. Here, the rule of mixtures and classical laminate theory is used to estimate the effective in-plane elastic modulus E1 and E2 for the given hybrid laminate composite. A simplified approach is assumed to calculate the average properties weighted by the thickness of each layer.[54]

$$E1_{Hybrid} = \frac{\sum_{i=1}^{n}(E1_i.t_i)}{h}. \quad (1)$$

$$E2_{Hybrid} = \frac{\sum_{i=1}^{n}(E2_i.t_i)}{h}. \quad (2)$$

According to the calculation above, $E1_{Hybrid} = 68.2\,GPa$ and $E2_{Hybrid} = 26.94\,GPa$. The significant difference between $E1_{Hybrid}$ and $E2_{Hybrid}$ indicates directional dependence of mechanical properties, which is a characteristic of orthotropic materials in which the fibers can be oriented in directions that maximize strength and stiffness where needed, improving overall structural performance.

	E_1 (GPa)	E_2 (GPa)	ν_{12}	G_{12} (GPa)	Thickness (mm)
Twill carbon	61.9	59.1	0.61	2.43	0.2
Glass UD	55	3.5	0.36	2.19	0.25
Carbon UD	107	7.6	0.33	3.02	0.25

TABLE 1 Mechanical properties of materials.

TABLE 2 Density and viscosity values for epoxy and hardener.

Material	Density (gr/cm^3)	Viscosity (mPas)
Hexion LR285 epoxy	1.18–1.23	600–900
Hexion LH287 hardener	0.94–0.97	80–120

During the manufacturing process of the composites, a weight ratio of 1:1 was maintained between the fibers and the matrix. The Hexion LR285 epoxy resin and Hexion LH287 hardener used had a weight ratio of 5:2, as shown in Table 2.

Prior to the composites' manufacturing, self-healing capsules were produced according to steps given in Figure S2. The procedure to produce self-healing capsules involves the deposition of urea-formaldehyde using in-situ polymerization. The present study involved the synthesis of microcapsules using bisphenol A (DGEBA) epoxy and chlorobenzene (PhCl) solvent as inducers. Due to its elevated viscosity ($\eta DGEBA$=1.3 Pas), epoxy cannot be alone covered with a solid shell. To reduce the viscosity of the epoxy, a non-polar solvent such as PhCl, with a viscosity of 0.75×10^3 *Pas*, is utilized. This solvent is carefully mixed with the epoxy (see Figure S1). PhCl has the dual effect of reducing viscosity and promoting the activation of the self-healing mechanism. Upon rupture of the microcapsule shell, the migration of PhCl toward the crack zone induces the activation of the amine groups (NH_2) present in that region, therefore commencing the epoxy curing reaction. Following the completion of the reaction, the solution containing microcapsules undergoes filtering and several washing with deionized water. After the completion of the cleaning procedure, the product is thereafter subjected to a drying period of roughly 48 hours under a fume hood. In order to achieve a thorough removal of any residual moisture from the microcapsules, an additional drying procedure can be performed for a period of 24 hours at a temperature of 30°C within a vacuum oven. The optical microscope is utilized to analyze the self-healing capsules that have been made by the aforementioned techniques. The capsules are submerged in silicon oil to facilitate the observation.

After the fabrication of self-healing capsules (see Figure S3), the composites outlined in Table 3 were manufactured. Concurrent with the manufacturing planning process, test cases are established to examine the distinct effects of the self-healing agent and SiC_w. The properties of the SiC_w (Hongwu®) used in this study is given in Table 3.

Test cases defined for hybrid laminated composites are conducted with four samples, and the details of each test case regarding self-healing agent, SiC_w, damage status, and curing are given in Table 4. In Case 1, no self-healing chemicals or SiC_w are introduced to hybrid composite specimens, and no damage generation to the specimens is anticipated. In Cases 2.1 and 2.2, 0.5 wt% SiC_w was included in hybrid composite specimens without a self-healing agent. In Case 3.2, 0.5 wt% SiC_w was added to the hybrid composite specimen with 5 wt% self-healing agents. Different from Case 1 and 2.1, in Case 2.2 and 3.2, specimens are subjected to 1 joule of impact energy to generate cracks. Additionally, in Case 3.2, specimens are cured for 16 hours at room temperature and 8 hours at 100°C.[30] Case 1 and Case 2.1 are established to examine the influence of SiC_w on the UTS in the undamaged composite. Cases 2.1 and 2.2 are formulated to assess the effect of damage on the UTS of the composite. Furthermore, Cases 2.2 and 3.2 are employed to ascertain the presence of the self-healing phenomenon in the composite material. Case 3.1 is employed primarily to examine the potential impact of post-curing by exclusively raising the temperature of composites that have previously been cured. The reason for this is that, during the initial cycle of composite polymerization in the vacuum-assisted resin transfer molding (VARTM) technology, certain epoxy groups may not fully polymerize. By raising the temperature, these unpolymerized groups are able to complete their cross-linking process.

Following the completion of manufacturing and test planning, composites were produced using the VARTM technique (see Figure S5). Glass/carbon fiber plies were manually laid at the specified angles illustrated in Figure 1. Afterwards, a mixture of epoxy resin and SiC_w was impregnated into the glass/carbon fibers with the application of vacuum pressure. Additionally, healing capsules were evenly distributed using a sieve with a mesh size of 300 μm between each layer in compositions containing healing agents. According to Figure 2A, the capsules that were produced have a spherical morphology, characterized by a diameter of around 100 μm.[55] As seen in Figure 2A, one of the self-healing capsules has a

TABLE 3 The properties of SiC_w material.

Product code	Color	Crystal form	Diameter (μm)	Length (μm)
D500B	Laurel-green	Cubic crystalloid	0.1–1	5–30

Density (g/cm^3)	Modulus (GPa)	Tensile strength (GPa)	Hardness (Mohs)	Temperature tolerance (°C)
3.21	480	20.8	9.5	2960

TABLE 4 Test cases for hybrid laminated composites.

Test case	Self-healing agent	SiC_w	Damage status	Curing
Case 1	No capsules	No SiC_w	Undamaged	No curing
Case 2.1	No capsules	0.5 wt%	Undamaged	No curing
Case 2.2	No capsules	0.5 wt%	1 J	No curing
Case 3.1	No capsules	0.5 wt%	1 J	Cured
Case 3.2	5 wt%	0.5 wt%	1 J	Cured

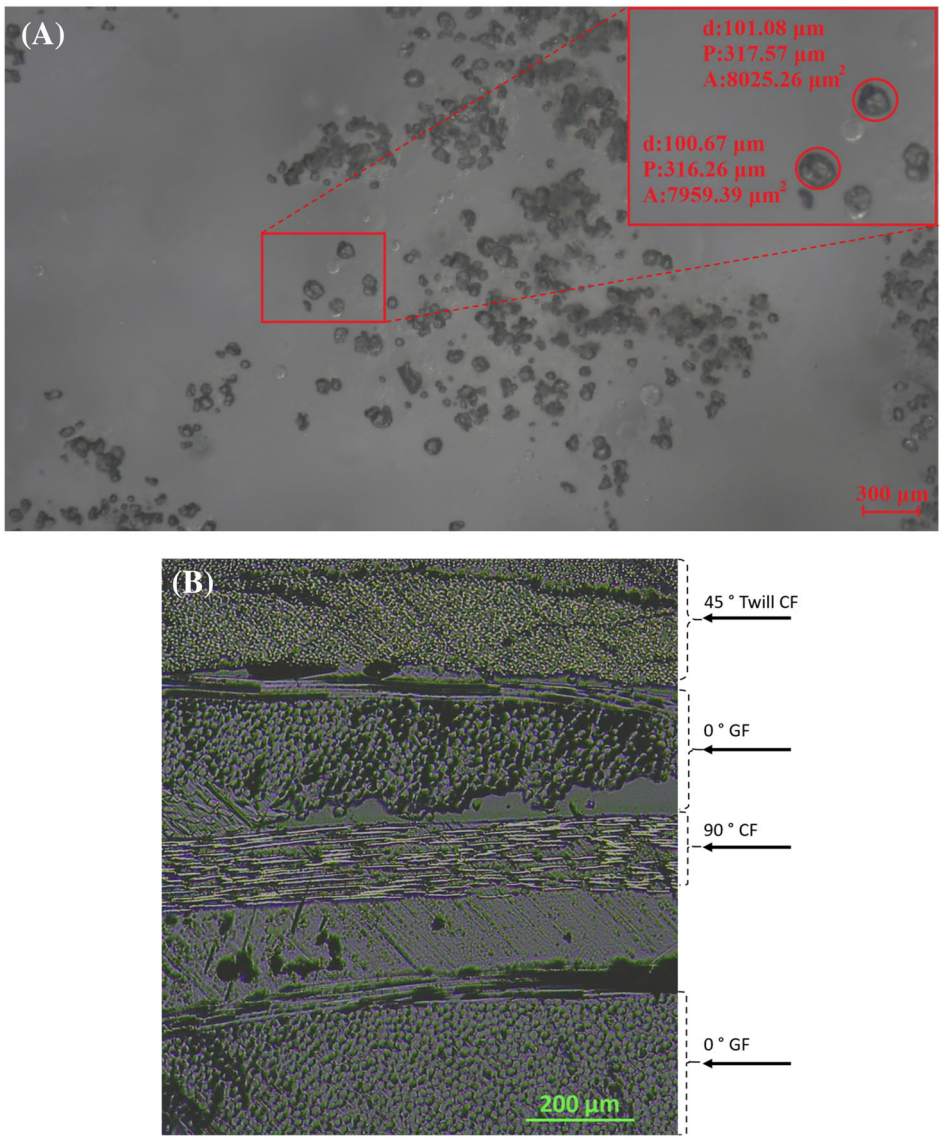

FIGURE 2 (A) Produced self-healing capsules; (B) microstructure of manufactured hybrid composite laminate.

diameter of 101.08 μm, a perimeter of 317.57 μm and an area of 8025.26 μm^2. The measured diameters of the highlighted capsules indicate a high degree of size consistency among the self-healing capsules. This consistency is beneficial for ensuring predictable performance in the composite material. Figure 2A reveals a relatively uniform distribution of the capsules throughout the observed area, is crucial for applications where homogenous self-healing properties are desired. Also, an area in Figure 2A is marked with red lines and represented separately to magnify specific parts of the figure. The magnified section of Figure 2A emphasizes the detailed structure of individual capsules, allowing for a closer examination of the capsule walls and any potential defects. This magnification highlights the structural integrity of the capsules, essential for their self-healing function. Once the curing process is finished, composites were obtained in plates (see Figure S6), from which specimens were extracted using abrasive water jet cutting. Following the manufacture of the composite, one of the tensile test specimens was sectioned, mounted, and polished in order to conduct a microstructural study. The use of an optical microscope allows for the observation of the different plies seen in Figure 2B. Figure 2B clearly shows the distinct layers of the hybrid composite which is crucial for the mechanical properties of the structure. Upon microscopic examination, no voids, fractures, or interface issues are identified. The absence of voids, fractures, or delaminations between the different layers indicates a strong interfacial bonding within the composite. This suggests that the manufacturing process was well-controlled, resulting in an optimized matrix-fiber adhesion that enhances the structural performance of the composite.

The quasi-spherical black structures, identified as self-healing capsules, are uniformly distributed within the matrix without disrupting the fiber alignment. This uniform distribution is essential for the effective activation of the self-healing mechanism, ensuring the composite maintains its integrity after damage. The consistent morphology of the capsules across different layers suggests a homogeneous dispersion process. This homogeneity is critical for reliable self-healing action throughout the entire composite, ensuring that damage can be addressed uniformly regardless of its location.

After the specimens were extracted from the composite plates, they were subjected to end-tabbing in order to prepare them for the tensile testing. The tabs are manufactured based on the specified measurements outlined in the standard, which include a thickness of 2 mm, a length of 56 mm, and a width equal to that of the specimen. Then, sample surfaces were prepared, and a strain gauge was attached to measure strain during tensile tests (see Figure S7). The ASTM D3039 standard has been employed for conducting tensile tests to ascertain the fundamental mechanical characteristics. Six rectangular specimens were prepared, and tensile tests were conducted with a Shimadzu AG-x 50 kN testing apparatus, employing a loading rate of 5 mm/min subsequent to the impact application. The elastic modulus, ultimate tensile strength (UTS), and strain at break were measured using tensile tests following the guidelines of ASTM D3039.[56]

Aside from mechanical testing, an evaluation of the tribological properties of the developed composites is conducted. Tribological tests were conducted on the Turkyus podwt wear test device using 320 grit sandpaper as given in Figure 3A. In addition, demonstrations of the sample holder and test sample were presented in Figure 3B. Lastly, views of the sample holder and test sample during the wear test were shared in Figure 3C. As can be seen from Figure 3B,C, the samples were replaced to the wear test machine via sample holder to ensure accurate testing. The wear test setup used for the tribological evaluation materials consists of several key components designed to simulate abrasive wear conditions. The test sample, prepared from the developed composite material, is subjected to controlled wear against abrasive sandpaper. The abrasive medium is securely mounted, ensuring consistent surface contact with the test sample throughout the experiment. Different test loads are applied using a manual control unit, which allows precise adjustment and monitoring of the load during the test. This setup replicates real-world conditions by ensuring constant pressure and surface interaction between the sample and the abrasive medium. The system is equipped with data recording software that continuously monitors and logs essential parameters such as friction force, wear rate, and displacement during the test. This comprehensive setup enables the accurate and repeatable assessment of the wear resistance and tribological behavior of the composite materials under study.

Test forces of 10, 20, and 40 N were selected for a duration of 2 minutes, with a test speed of 2 m/s. Friction force data generated during the tests were recorded using Esit Data Logger 1.1.8 software.

The specimens for the tribological assessment are prepared as given in Figure 4. The weights of each sample were measured before and after the abrasion test using a Radwag AS/220/C/2 precision balance, and weight losses were calculated. Weight losses were also determined by dividing them by the density values of the samples to ascertain volume losses. Furthermore, the surface roughness values of the samples were determined before and after wear at varying loads using a surface profilometer (Mahr MarSurf PS1). Additionally, the worn sample surfaces were examined with an optical microscope (Nikon SMZ800 [Tokyo, Japan]) cooperates with Dpx View software.

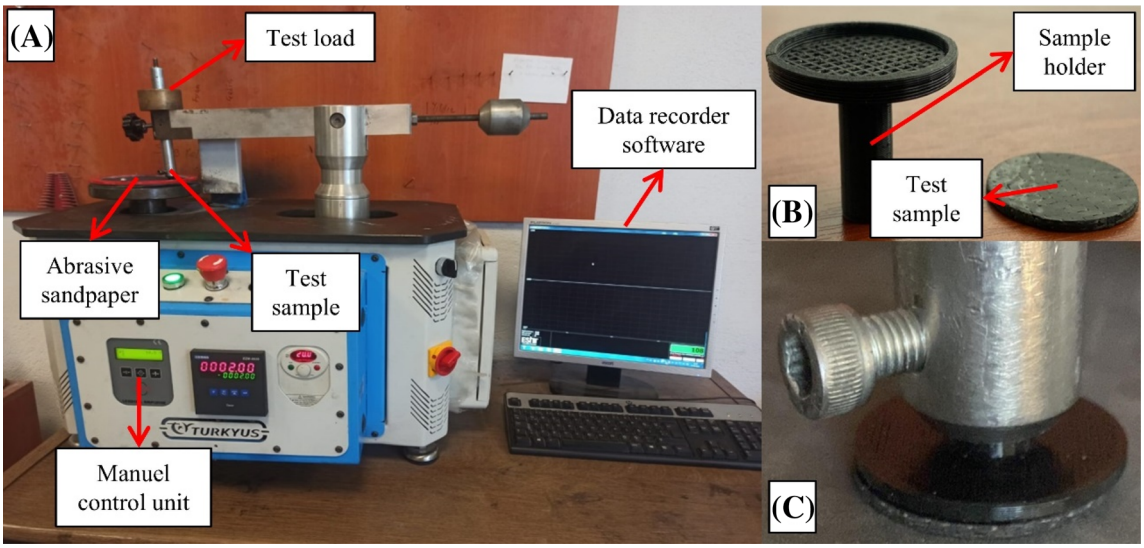

FIGURE 3 Wear test setup, (A) equipment of the wear test machine, (B) demonstration of the test sample and sample holder, and (C) view of the test sample and sample holder during the wear test.

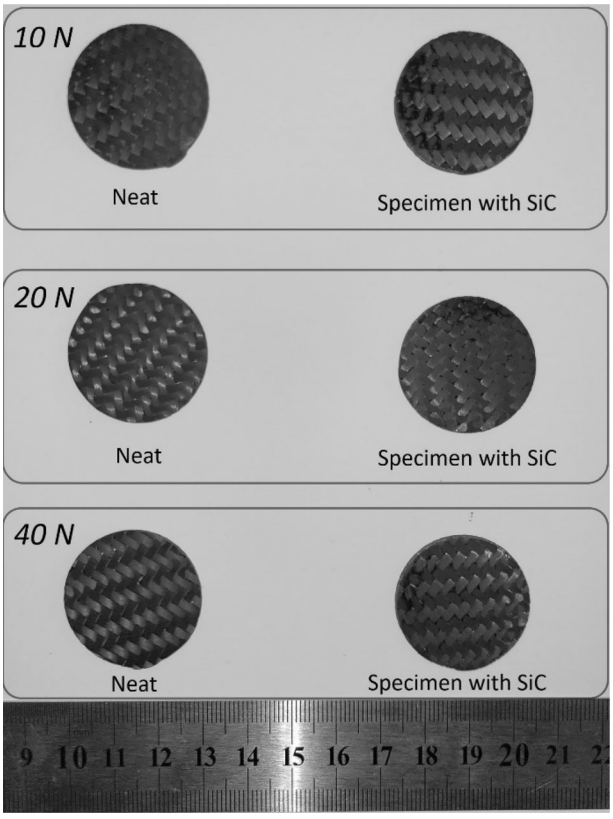

FIGURE 4 Specimens for tribological assessment.

3 | THEORETICAL BACKGROUND FOR BIRD STRIKE INTERPRETATION

The current study focuses on the impact characteristics of a hybrid laminate composite and its capacity for self-healing through microcapsules, particularly in the context of bird strike-induced damage. The objective of this section is to provide a theoretical framework that seeks to clarify the process of damage resulting from bird attacks and determine the amount of energy required for conducting impact tests.

3.1 | Evolution of stress by bird strike damage

Bird strikes pose a significant risk to composite structures such as wind turbine blades. The transfer of kinetic energy that occurs upon impact initiates various forms of damage, such as crack initiation and propagation, fiber damage, and delamination. These incidents weaken the structure, leading to matrix cracking, fiber fracture, and potential structural failure. Understanding these causes of damage is essential for creating resilient composite structures that can endure bird hits. This knowledge may guide the choice of materials, structural design, and maintenance methods to improve the safety of aircraft and wind turbines.

When a bird collides with a composite structure, it transfers its kinetic energy to the structure. This sudden energy transfer can cause localized deformation and stress concentrations at the point of impact. Then, damage initiation observed with several local issues, including matrix and fiber fracture, manifested themselves in composite laminates prior to their ultimate failure.

When a damage initiation criterion is met, continued loading leads to the degradation of the material's stiffness coefficients. The material exhibits linear elasticity up to a

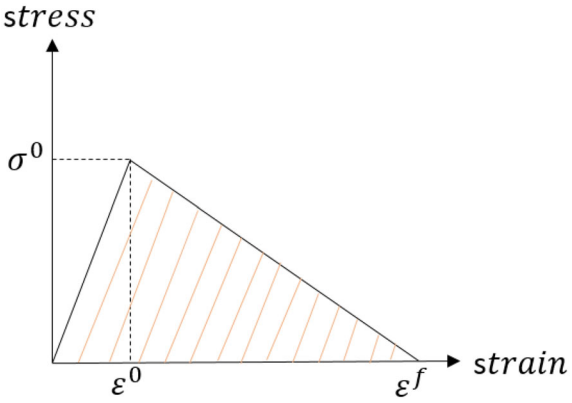

FIGURE 5 Stress–strain diagram for softening material.

TABLE 5 Equivalent strain and stress for different failure modes.[57]

Failure mode	ε_{eq}	σ_{eq}
Fiber tension	$L_e\sqrt{(\varepsilon_{11})^2+\alpha(\varepsilon_{12})^2}$	$\frac{L_e[\sigma_{11}\varepsilon_{11}+\alpha\sigma_{12}\varepsilon_{12}]}{\varepsilon^f_{eq}}$
Fiber compression	$L_e(-\varepsilon_{11})$	$\frac{L_e[(-\sigma_{11})(-\varepsilon_{11})]}{\varepsilon^f_{eq}}$
Matrix tension	$L_e\sqrt{(\varepsilon_{22})^2+(\varepsilon_{12})^2}$	$\frac{L_e[\sigma_{22}\varepsilon_{22}+\alpha\sigma_{12}\varepsilon_{12}]}{\varepsilon^m_{eq}}$
Matrix compression	$L_e\sqrt{(-\varepsilon_{22})^2+(\varepsilon_{12})^2}$	$\frac{L_e[(-\sigma_{22})(-\varepsilon_{22})+\alpha\sigma_{12}\varepsilon_{12}]}{\varepsilon^m_{eq}}$

peak stress value, followed by linear softening in the post-peak phase, as shown in Figure 5.

The material's response following the damage initiation is distinguished by a progressive decrease in its stiffness. The reduction in material's stiffness is governed by damage variables, which can range from zero (representing an undamaged state) to one (indicating a fully damaged state for the associated mode). To account for the decreasing impact of element size as the material softens, a characteristic length for an element (L_e) is introduced in the equations for equivalent strain (ε_{eq}) and stress (σ_{eq}). Equivalent strain and stress are defined for different failure modes as given in Table 5.

ε^f_{eq} and ε^m_{eq} indicates the equivalent strain at which complete fiber and matrix failure of the material take place, respectively ($d_I = 1$). In order to preserve the correlation between equivalent stress and equivalent strain, the selection of the involved damage variable through the progression of damage evolution may exhibit variability. Once damage initiation occurs (i.e., when $\varepsilon_{eq} \geq \varepsilon^0_{eq}$), Equation 3[57] yields the specific damage variable denoted as "d_I" for a given mode.[57]

$$d_I = \frac{\varepsilon^f_{eq}\left(\varepsilon_{eq}-\varepsilon^0_{eq}\right)}{\varepsilon_{eq}\left(\varepsilon^f_{eq}-\varepsilon^0_{eq}\right)}. \tag{3}$$

The variable "d_I" denotes the equivalent strain at which damage initiation occurs. The determination of the specific value ε^0_{eq} for each damage mode is contingent upon the elastic characteristics and strength of the material, and it aligns with the stress levels established by the initiation criterion. There exists a relationship between equivalent strain and stress where the effective stress tensor emerges from the nominal stress tensor, and it is accompanied by a damage operator tensor that includes three internal damage variables (d_f, d_m, d_s) representing fiber, matrix, and shear damage, respectively. The damaged material's response is determined using Equation 4, and this calculation is employed to examine the gradual reduction in the stiffness of the composite layer, allowing for continuous tracking of damage progression.[57]

$$\sigma_{ij} = C_{ijkl}\varepsilon_{kl}, \tag{4}$$

where C_{ijkl} is the stiffness tensor upon damage and defined as follows:

$$[C_{ijkl}] = \frac{1}{D}\begin{bmatrix} (1-d_f)E_1 & (1-d_f)(1-d_m)\nu_{21}E_1 & 0 \\ (1-d_f)(1-d_m)\nu_{12}E_2 & (1-d_m)E_2 & 0 \\ 0 & 0 & (1-d_s)GD \end{bmatrix}. \tag{5}$$

$$D = 1-(1-d_f)(1-d_m)\nu_{12}\nu_{21}. \tag{6}$$

In Equations 5 and 6, E_1 corresponds to the Young's modulus along the fiber direction, E_2 represents the Young's modulus in the direction perpendicular to the fiber orientation, G denotes the shear modulus, and ν_{12} and ν_{21} refer to the Poisson's ratios. The progression of the damage variable after initiation is determined by the fracture energy (G_f) released during the damage process.

$$\varepsilon_{eq}^{f} = \frac{2G_f}{\sigma_{eq}^{0}}. \tag{7}$$

3.2 | Translation of energy for bird strike interpretation

The provided formulation (see Equation 5) relies on a representative unit volume and considers energy dissipation within this volume. However, it is necessary to characterize cracks and their propagation by quantifying the energy needed to expand the fractured area or cracked surface. Hence, it is essential to develop a correlation between fracture mechanics and damage mechanics. The dissipation of specific fracture energy (E_f) can alternatively be mathematically represented as follows[58,59]:

$$E_f = \int_0^{\infty} \sigma_{ij} d_I \varepsilon_{ij}. \tag{8}$$

This corresponds to the region under the stress–strain curve. The specific energy dissipated can be divided into two components: the elastic energy, denoted as E_e, and the propagation energy, referred to as E_p. This relationship gives rise to the subsequent equation:

$$E_f = E_e + E_p. \tag{9}$$

By merging damage and fracture mechanics techniques, the energy dissipated can be directly linked to the energy required for failure, which should be inherent to the material and specific to each failure mode. The term "intralaminar fracture energy" refers to the amount of energy dissipated per unit area. Here, the energy dissipated per unit area is often termed the intralaminar fracture energy (G_f): Here it is assumed that damage related to delamination primarily happens exclusively at the interface.

$$G_f = \int_0^{\infty} \sigma_{ij} d_I \delta_{ij}. \tag{10}$$

The energy spent within a volume element V_e and the fractured area A_e is characterized as follows:

$$\left(E_e + E_p\right) V_e = G_f A_e. \tag{11}$$

For a characteristic length for an element, which is defined as:

$$L_e = \frac{A}{l}. \tag{12}$$

In this context, "l" represents the greatest dimension of the area element A. Therefore,

$$\left(E_e + E_p\right) A_e L_e = G_f A_e. \tag{13}$$

Rearranging the equation above, yields,

$$E_p = \frac{G_f}{L_e} - E_e. \tag{14}$$

The dissipation of energy should exhibit independence from the size of the element. By maintaining a constant specific internal energy, it is possible to calculate the corrected value of E_p for various element sizes. The specific energy of a bilinear stress–strain-damage curve can be simply described as:

$$E_f = \frac{1}{2}\sigma_0 \varepsilon_{max}. \tag{15}$$

$$E_p = \frac{1}{2}\sigma_0 (\varepsilon_{max} - \varepsilon_0). \tag{16}$$

$$E_e = \frac{1}{2}\sigma_0 (\varepsilon_0). \tag{17}$$

The intralaminar fracture energy associated with tensile or compression failure can be quantified using compact tension and compact compression specimens. The intralaminar fracture energy, a term derived from fracture mechanics, can be utilized to determine the energy released within the finite element volume due to associated damage and fracture mechanics. The energy dissipated for a particular damage mode, and the relationship between damage and fracture mechanics is defined as[58,59];

$$\Pi = \left(E_e + E_p\right) A L_e. \tag{18}$$

Numerous studies have been conducted to investigate the effects of bird strikes on composite plates and the subsequent structural damage. Table 6 outlines the experiments undertaken with various levels of kinetic energy, bird mass, and specimen size. The energy dissipation is correlated with the dimensions of the specimen, specifically the longest length, specimen area, or fracture area, as seen by Equation 18. Hence, relevant information has been reported in Table 6 according to research findings.[60,61]

Analyzing the experimental applications suggests a relationship between kinetic energy, characteristic length, and specimen area, as shown in Figure 6. This relationship

TABLE 6 Examples for impact analysis applications with high and low velocity.

Case	Kinetic energy	Mass (kg)	Velocity (m/s)	A, Fracture area (mm^2)	A_e Specimen area (mm^2)	L, longest length (mm)
Case 1[60]	30,000 J	1	245	75,000	375,000	750
Case 2[60]	10,800 J	1	147.5	27,000	375,000	750
Case 3[61]	9.7 J	2.82	2.61	190	7853.98	100
Case 4[61]	5 J	2.8	1.89	108	7853.98	100
Case 5	1 J	0.167	3.46	97	3750	250

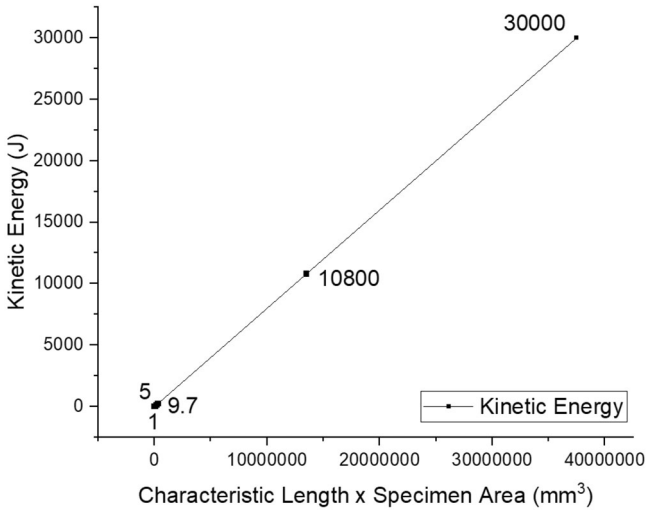

FIGURE 6 Relationship between kinetic energy, characteristic length, and specimen area.

is analogous to the energy dissipation formula given in Equation 18.

The York approach was employed to conduct linear regression analysis with X error on five separate examples as presented in Table 6. The findings of this analysis are illustrated in Figure 6. The linear regression results given in Table 7 demonstrate that the slope of 8.0004E-4 establishes a statistically significant correlation between kinetic energy, characteristic length, and specimen area. The standard error associated with this relationship is calculated to be 3.06569E-8.

According to Figure 7, the kinetic energy and standard residuals for five different scenarios have been determined. The differences between the predicted and actual values of the dependent variable, as calculated by the statistical model, are illustrated in Figure 7 through the use of standard residuals. In addition, the percentiles depicted in Figure 7 allow for visualizing the distribution of the data and identify the specific positions of individual data points within the dataset that includes the five distinct scenarios.

The impact energy required for the test specimens, measuring 15 mm × 250 mm, has been calculated to be 1 J, taking into account the characteristics of the specimens. Yet, previous studies have demonstrated that including twill textiles into the outer layers of the composite lay-up significantly improves the impact resistance of the composite material.[62–64]

Bird strikes are an important aspect of wind turbine design since it allows us to understand how the structure responds to impact damage. Thus, this article used the Charpy impact test to mimic the wind turbine's response against bird impacts. Charpy impact tests were performed using the Zwick Roell HIT5P Universal Charpy tester. Furthermore, bird strikes should be simulated in an ex-situ scenario using factors such as the bird's speed and weight. The EASA Standard[65] proposes a bird weight of 1.8 kg (4 lbs). A striking bird, on the other hand, is estimated to fly at 11.4 m/s based on wind assumptions.

4 | RESULTS AND DISCUSSIONS

4.1 | Effect of SiC whiskers and self-healing capsules on mechanical performance

Initially, the study focused on investigating the impact of SiC_w whiskers on mechanical characteristics by conducting experiments using two cases, Case 1 and Case 2.1, as shown in Table 8. Furthermore, the effectiveness of the self-healing capsules was investigated in the other cases. The tests yield data for the UTS, as shown in Table 8 (and also in Table S1, Figures S8 and S9 for each specimen).

According to Table 8, the incorporation of 0.5 wt% SiC_w leads to a significant enhancement of 32% in the UTS of the composite material. The observed phenomenon can be ascribed to the presence of whiskers, which can provide supplementary mechanisms for enhancing the strength of the composite material.[66] These mechanisms include fiber/whiskers/matrix bridging and whisker pull-out. Additionally, it has been suggested that the presence of rough textured whiskers might enhance the adhesion between the matrix and the whiskers, hence preventing premature displacement of the matrix phase. This, in turn,

TABLE 7 Statistics summary for linear fitting of kinetic energy—characteristic length × specimen area.

	Intercept		Slope		Statistics
	Value	Standard error	Value	Standard error	Adj. R-square
Kinetic energy	−1.24555	0.54643	8.0004E-4	3.06569E-8	1

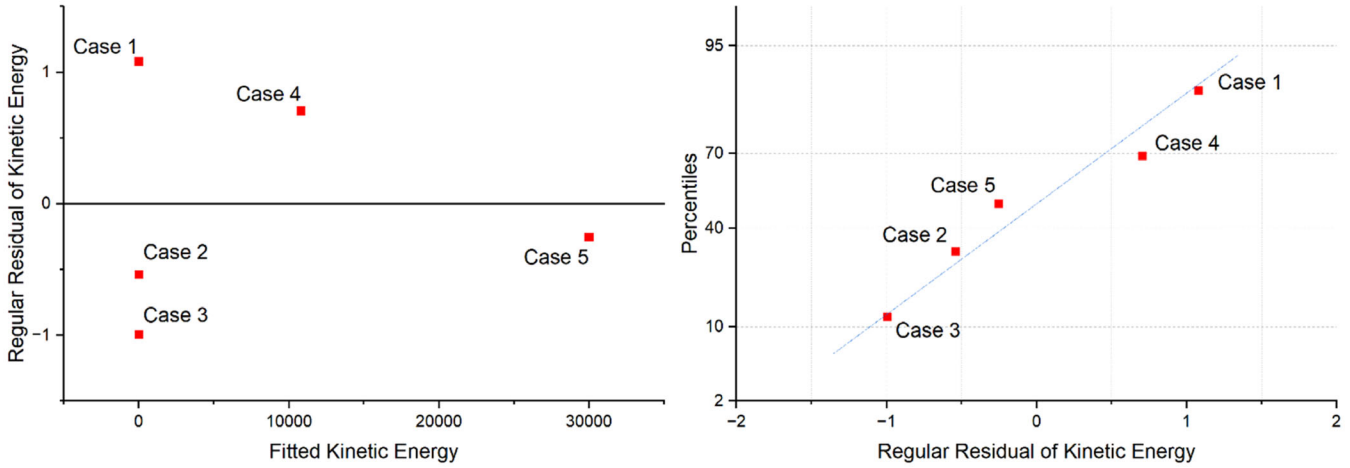

FIGURE 7 Fitted curves plot.

TABLE 8 Tensile test results of hybrid laminated composite.

Case #	wt% self-healing	wt% SiC_w	Damage condition	UTS (MPa)
Case 1	0	0	Undamaged	237.90 ± 3.12
Case 2.1	0	0.5 wt% SiC_w	Undamaged	313.21 ± 5.28
Case 2.2	0	0.5 wt% SiC_w	1 J (damaged)	283.37 ± 4.49
Case 3.1	0	0.5 wt% SiC_w	1 J (damaged)	285.87 ± 1.12
Case 3.2	5 wt%	0.5 wt% SiC_w	1 J (damaged)	298.87 ± 3.17

leads to a significant increase in the UTS, stiffness, flexural strength, and modulus of the material.[50,67–69]

After conducting an analysis of the effect of reinforcements, particularly through a comparison of cases 2.1 and 2.2, it becomes apparent that 1 J impact damage in the composite material leads to a reduction of around 30 MPa in the UTS. The observed decline in UTS indicates a 10% decrease in comparison to the undamaged condition. On the other hand, the comparison of Cases 2.2 and 3.2 is used to determine the effect of self-healing capsules on the composite structure. After describing the process of impact damage formation and the subsequent healing cycle in the methods section, the efficiency of self-healing was examined. The data shown in the third and fifth rows of Table 8 indicates a significant rise of 15 MPa in the UTS. This outcome is directly related to the self-healing agents' recovery. When impact-damaged capsules are torn, the unpolymerized thermoset resin is released and diffuses throughout the thermoset matrix, filling the cracks that may have formed as a result of the impact. The resin subsequently performs a curing reaction with the unused amine groups that were present within the cracks. The curing process is completed gradually by applying heat, effectively repairing the microcracks.

As given in Section 3, composite structures can experience low or high velocity impacts like bird strikes which are interpreted as significant damage to the structure's behavior. Here, the energy required to propagate a crack is a key measure of the material's toughness and therefore, the effectiveness of self-healing capsules becomes more significant in this process. These healing agents fill the cracks and initiate polymerization, bonding the damaged area and restoring mechanical properties (which is explained with reduction in specific damage variables) even if the full recovery of the tensile strength is not possible, as seen in Table 8. However, the integration of self-healing capsules improves the tensile strength of the structure,[29] which enhances their ability to recover from damage, thereby improving the durability of the structure.

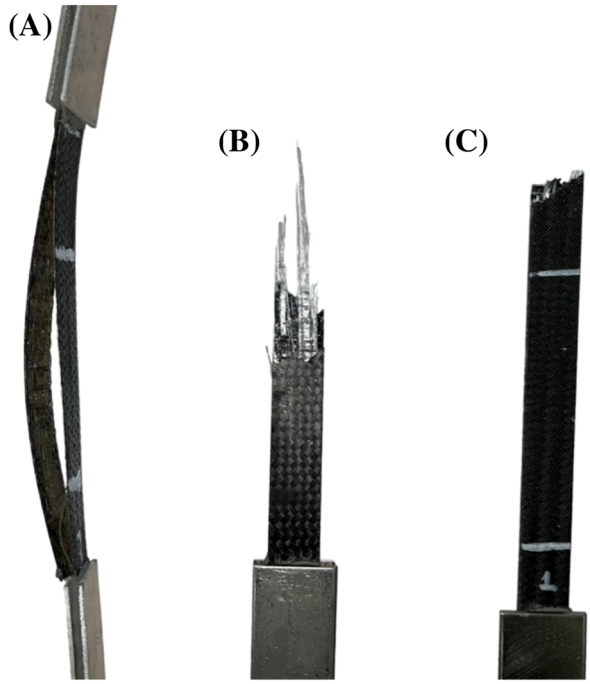

FIGURE 8 Post-mortem images of tensile test specimens.

4.2 | Damage observation on a macroscopic scale

The laminate composites display diverse damage mechanisms, offering insights into their damage behavior relative to the structural mechanical properties. As depicted in Figure 8, various damage mechanisms can be observed in the developed composite specimens.

Figure 8A depicts the fundamental damage mechanism as delamination. Delamination is a phenomenon characterized by the separation of layers inside laminated composite materials, resulting from the persistent application of stress on the material as well as the low interfacial strength. This delamination issue could result in poor performance. Insufficient curing procedures produce unequal pressure on various areas, leading to the formation of delamination zones. The formation of delamination zones in composite materials can significantly reduce the strength of the composite when subjected to external stresses. Delamination can arise from manufacturing faults or external factors that affect composite laminates over time, such as the presence of foreign objects.[70–72] A fracture in the fiber can be observed in Figure 8B, which extends in a direction parallel to the force that was applied. The glass fibers are depicted in Figure 1 at an angle of 0°, indicating that they are anticipated to support the primary tensile load throughout the tensile test. When the tensile strength of the glass fibers is surpassed in certain regions during the tensile tests, failure happens, and the residual load is attempted to be sustained by the remaining fibers. However, the inadequate transverse strength of glass fibers prevents them from effectively supporting burdens. Subsequently, the composite undergoes a gradual deterioration, culminating in the total failure of the specimen. The discernible discrepancy in the ultimate lengths of the various plies, as illustrated in Figure 8B, provides visual confirmation of this mode of failure. As shown in Figure 8C, the absence of delamination provides conclusive evidence that the fracture zone is sufficiently protected. It is hypothesized that simultaneous matrix and fiber degradation occurred subsequent to achieving a particular stress threshold. The failure of the matrix potentially led to a reduction in the effective stress transfer. As a consequence, the dominant fiber plies experienced an inadequate transfer of tension, which ultimately caused fiber breakage in the succeeding layers. Consequently, a significant amount of load was attempted to be borne by a single ply. However, the inadequate ply strength resulted in a sudden and complete collapse of the test specimen.[73–77]

TABLE 9 Charpy impact test cases.

Cases	Self-healing agent	wt% SiC_w
Case 1	No capsules	No SiC_w
Case 2	No capsules	0.5 wt% SiC_w
Case 3	5 wt% self-healing capsules	0.5 wt% SiC_w

4.3 | Impact behavior of composite with self-healing capsules and SiC_w

After assessing the effectiveness of the self-healing mechanism, the impact resistance of the composite is examined using Charpy impact experiments. The specific test cases are defined with four samples and the results are given in Table 9 (see Figure S10 for the result of each sample).

The Charpy impact test results indicate that Case 1, which pertains to the specimen without self-healing capsules, has a value of 75.30 kJ/m^2 (see Figure 9). According to Figure 9, the addition of 0.5 wt% SiC_w to the hybrid composite material results in a 45% increase in its energy absorption capacity, reaching 109.75 kJ/m^2. As mentioned earlier, the inclusion of SiC_w whiskers inside the structure adds an extra phase to the matrix, hence improving the interaction between the fiber, matrix, and whiskers. In addition, whiskers can serve as ropes, thereby holding both ends of a crack. As a result, in order to fully propagate the pre-existing notch, the system requires additional energy.[50]

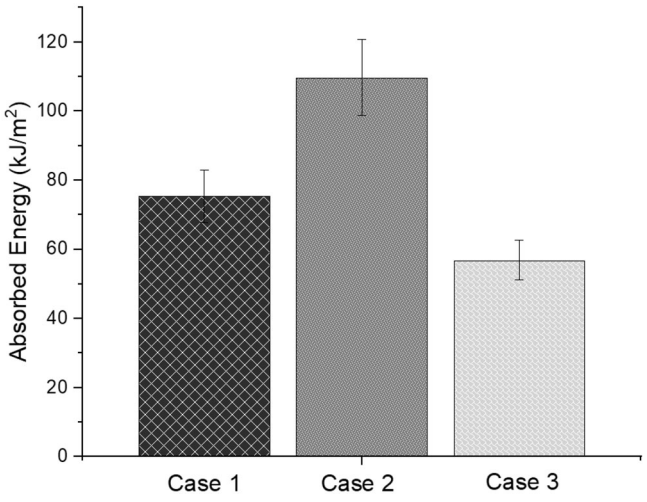

FIGURE 9 Absorbed energy results of different test cases.

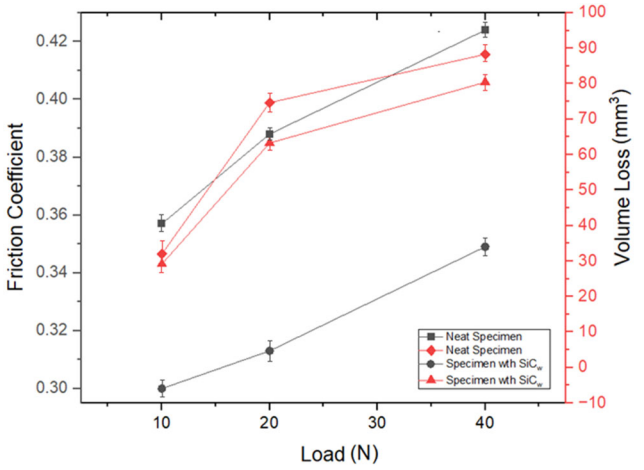

FIGURE 10 Measurement of volume loss and friction coefficient under varying load.

On the other hand, the inclusion of 5 wt% self-healing agents reduces the energy absorption capacity of the material. These capsules in the microstructure constitute the weak points of the matrix, like quasi-voids. Due to these weak points, stress concentration occurs upon impact, and total failure is observed well before the composite without self-healing capsules. Last but not least, the reduction in absorbed energy in Case 3 can also be attributed to increased interlaminar thickness due to the size and concentration of microcapsules and catalyst dispersion.[36]

4.4 | Tribological assessment of the developed composites

4.4.1 | The impact of SiC_w on the wear resistance of laminated composites

An analysis of the wear characteristics of the composite specimens was performed in accordance with the guidelines described in the ASTM G99 standard.[78] To analyze wear behavior, abrasive paper with a mesh size of 320 was used. The specimens were subjected to abrasion testing at varying forces of 10 N, 20 N, 30 N, and 40 N, with a speed of 2 m/s and a two-minute timeframe.

The principal key contributing to increased wear in fibrous composites is the act of fiber detachment and debonding. As the composite surface slides dry, the majority of the applied load is borne by the fibers; consequently, fiber-rich regions experience interfacial fatigue and eventual debonding. In addition, dry sliding induces substantial friction and microplowing in the matrix, which intensify progressively following the peeling of the fibers. Ultimately, this causes matrix fracture and additional debonding between the reinforcement and matrix. The main factors that determine wear characteristics in composite materials are matrix fracture, fiber breaking, and fiber debonding. In the direction of dry sliding, the composite surface develops cracks and a small degree of matrix fracture. The marginal deformation observed on the surface of the composite emphasizes the substantial influence that particle size has on the wear characteristics of the composite. The presence of damaged or detached fibers increases fiber detachment from the matrix, reducing wear resistance. During sliding, the matrix region appears to rapidly deform and soften, which further reduces the resistance to wear and initiates debonding between the reinforcement and matrix. Drawing from the aforementioned observations, it is possible to deduce that the SiC_w-reinforced composite exhibits an enhanced resistance to wear in comparison to the neat composite.[79,80]

The SiC_w hybrid composite exhibited superior wear resistance under varying loads. A higher rate of wear is observed in the early stage, mainly due to the interaction between the less resilient epoxy resin and the abrasive sandpaper. Figure 10 demonstrates that at a load level of 20 N, the hybrid composites containing SiC_w experience a volume loss of 63.27 mm^3, whereas the neat hybrid composites demonstrate a volume loss of 74.64 mm^3. Furthermore, as an example, when subjected to a load of 40 N, the hybrid composites, including SiC_w experience a volume loss of 80.42 mm^3, whereas the neat hybrid composites undergo a volume loss of 88.28 mm^3. The enhanced performance can be attributed to the presence of SiC_w particles on the opposite surface, which successfully withstands plastic deformation and serves as a robust barrier against extensive fragmentation. As a result, the amount of wear in the neat hybrid composite is significantly more than in the hybrid composites, including SiC_w. The enhanced wear resistance of the hybrid composite containing SiC_w can be attributed

to the unique properties of SiC_w, which consist of tetrahedral carbon and silicon atoms that are tightly bonded in a resilient lattice structure. This particular arrangement results in a material that exhibits exceptional resilience and robustness, hence enhancing the strength of the composite. The hybrid composite incorporating SiC_w exhibits exceptional wear resistance and improved mechanical properties, highlighting the positive impact of SiC as a filler.

On the other hand, the neat hybrid composite exhibits greater wear loss in every scenario. The wear loss of the hybrid composite containing SiC_w exhibits an upward trend when the applied loads are increased. This is due to the energy barrier created on the specimen's surface, which is more substantial thanks to the incorporation of SiC_w particles into the matrix. Consequently, even at higher loads, the energy generated by third-party particles on the opposing surface is insufficient, resulting in limited penetration into the matrix material. Instead, a microfracture of the matrix material occurs, creating a transfer layer. The wear data for these composites clearly indicates that wear loss is heavily influenced by the applied load. Compared to the neat hybrid composites with SiC_w, the hybrid composites with SiC_w exhibit a lower specific wear rate under all conditions. This reduction in specific wear rate is attributed to the use of a thermoset matrix and the incorporation of SiC_w, which serves as a very efficient reinforcement for preventing wear.[81]

4.4.2 | The influence of SiC_w on the friction coefficient of the developed composites

The primary mechanism for dissipating frictional energy involves the shearing of an ultrathin zone, measuring only a few nanometers in thickness, at the composite interface. In cases where this sheared composite layer is deposited onto the smooth counter surface, it functions as a transfer layer, and subsequently, most of the frictional energy dissipation occurs within this transfer film or an extremely thin layer. The thin layer that detaches from the matrix comes into direct contact with the counter surface.[41,81]

The hybrid composite containing SiC_w exhibits a lower coefficient of friction compared to the neat hybrid composite. Furthermore, this coefficient of friction rises as larger loads are applied. According to the data presented in Figure 10, when subjected to a stress level of 20 N, the friction coefficients for the hybrid composite containing SiC_w and the neat hybrid composite are 0.32 and 0.39, respectively. In addition to that, as an example, at a load level of 40 N, the friction coefficients are 0.34 and 0.42 for hybrid composite with SiC_w and neat hybrid composite, respectively. This finding suggests that the hybrid composite containing SiC_w has a frictional advantage of around 20% compared to the neat hybrid composite. The study[82] demonstrates that the inclusion of silicon in the composite matrix has a substantial effect on the shape of the third body, resulting in adhesive friction and therefore reducing wear.

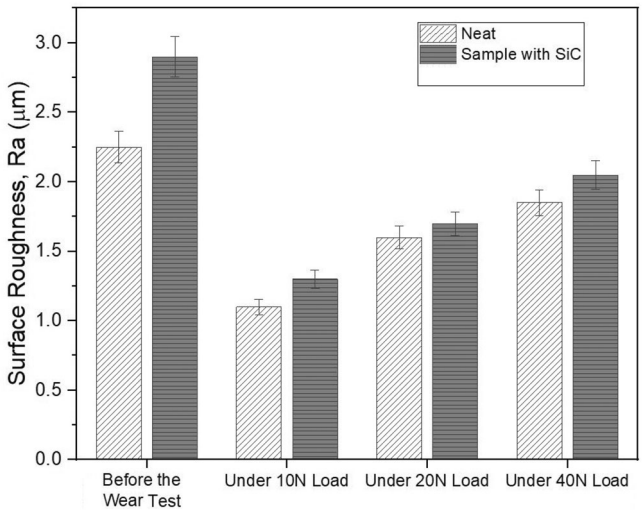

FIGURE 11 Surface roughness of the samples under different conditions.

Figure 11 presents the surface roughness values of the samples under different conditions. As illustrated in Figure 11, the surface roughness values of the samples with SiC were found to be higher than those of the neat samples across all conditions. This observation may be attributed to the presence of fillers. Moreover, the surface roughness values of 2.26 μm (SD: 0.28) and 2.94 μm (SD: 0.34) were reduced to 1.11 μm (SD: 0.086) and 1.26 μm (SD: 0.098) when the wear test performed under 10 N, respectively, for the neat and SiC-containing samples. As the abrasion test load increased from 10 to 40 N, it was determined that the surface roughness values exhibited a corresponding increase, contingent on the presence and extent of wear marks.

Figure 12 shows the optical images of the worn surfaces of neat samples and sample with SiC. Upon examination of Figure 12, it becomes evident that the number of wear lines increases in conjunction with the rise in test force, from 10 to 40 N. Additionally, it can be observed that the presence of wear lines is more pronounced in the neat sample than in the sample containing SiC.

4.5 | The industrial aspect of the developed composites

After completion of the tribological assessment of the developed composites, it is significant to assess the applicability of these materials to industrial structures, which

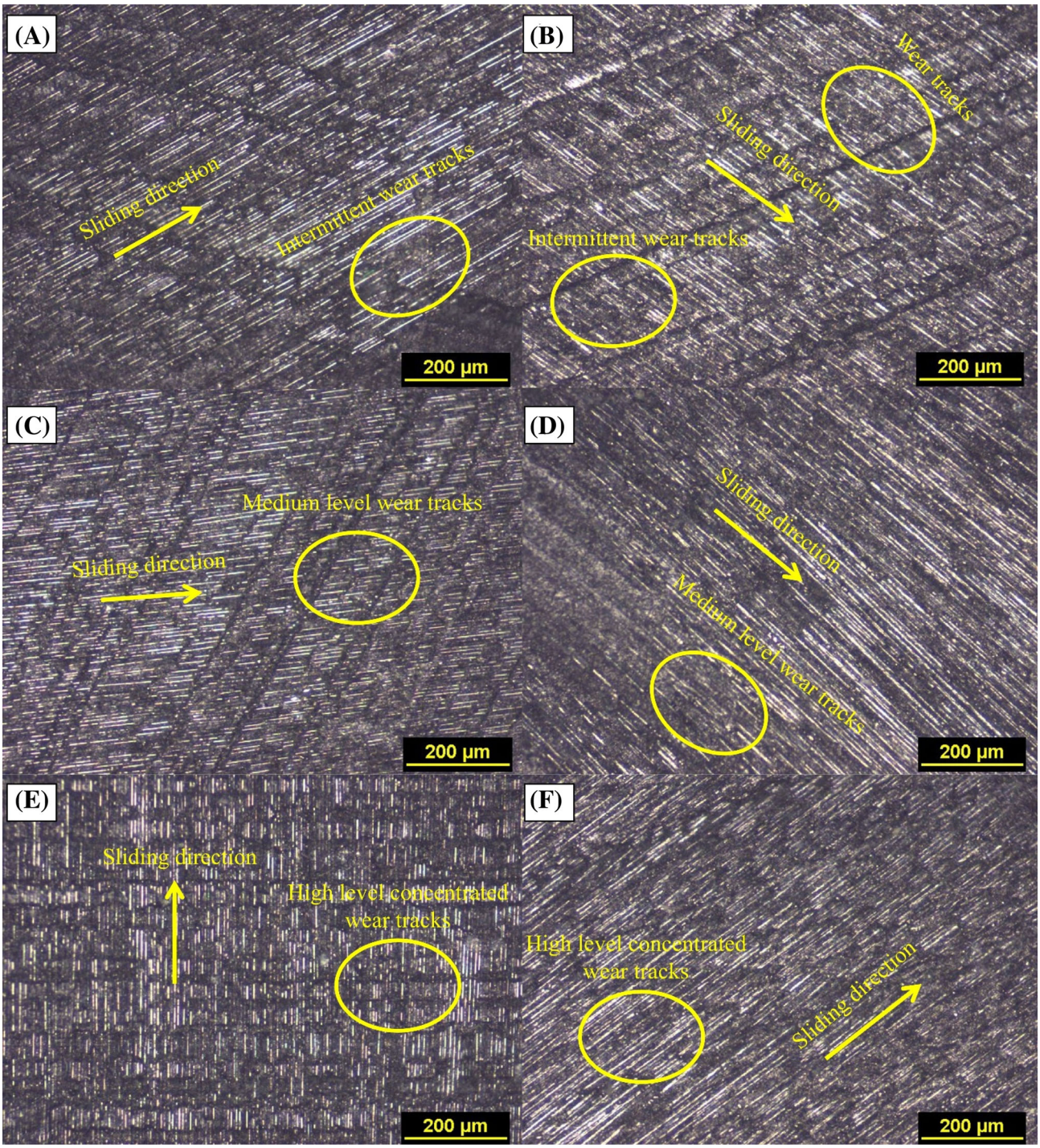

FIGURE 12 Optical images of the worn surfaces under different loads, (A) neat sample under 10 N, (B) sample with SiC under 10 N, (C) neat sample under 20 N, (D) sample with SiC under 20 N, (E) neat sample under 40 N, and (F) sample with SiC under 40 N.

leads to an estimation for the comparison with the composite design currently employed by the industry and the developed composite as part of this study. When overall self-healing addition process to composite is considered, it is not challenging to procure raw materials to prepare self-healing capsules. Moreover, the self-healing manufacturing process does not impact composite production since self-healing capsules are prepared separately before adding to composite layers. Here, the significant point is to evenly distribute capsules on the layers with a sieve, as explained in the materials and methods section. The addition of the capsules to composite layers was conducted manually in the laboratory by sieve which may have caused to be unevenly distributed on the layer and may have led to

TABLE 10 Cost comparison for neat composite and composite with self-healing.

Item	No self-healing	Self-healing
Production of the plate	$1427.4	$1427.4
Production of 60 g self-healing capsules	–	$309.27
Engineering cost	$1427.4	$1427.4
Material cost	$637.27	639.07
Total cost	$3492.07	3803.14

different capsule ratios in different portions of the layers. Therefore, autonomous manufacturing systems can be developed in the wind industry for self-healing capsules, and even these autonomous systems can be used for the distribution of capsules on each layer during the manufacturing of wind turbine blades. Another significant aspect for the wind turbine industry is the cost of such a developed composite structure. Table 10 shows the cost comparison of composite plates with and without self-healing.

As given in Table 10, the cost assessment includes the manufacturing, engineering, and material costs of the developed composites. When the cost is compared for composite plates, the main difference is obtained from the production of self-healing capsules. Even if there is no big impact in terms of material cost for self-healing capsules, the production of 60 g self-healing capsules is adding $309.27 as labor cost which means 8.85% extra cost for composite structures. When the weight ratio of self-healing is considered as 5 wt%, it leads to that the self-healing cost is $257.72 per kg of a composite structure. Although the cost of self-healing during manufacturing may seem high, but self-healing capsules may reduce the maintenance costs by healing the microcracks damage throughout the life cycle of wind turbine blades. As part of the industrial aspect of the developed composites, it is also significant to consider the industrial evaluations. The American Clean Power Association (ACP) states that self-healing is one of the proactive methods for more durable wind turbine blades, which prevents degradation and increases the service life of the blades.[83] Also, one of the strategic consulting companies for renewable energy mentioned in their report that operation and maintenance costs are 25% of the life cycle cost of an offshore wind turbine and as an example, the average cost of hiring a crane vessel to repair an offshore blade is £100,000 per day. Therefore, they suggest reducing the risk of blade failure by improving the structure, such as using self-healing composites.[84] When the industrial assessments are considered, it becomes more clear that self-healing composites are the key developments for the improved structures, and they also help reduce maintenance costs.

5 | CONCLUSION

The effects of self-healing agents and SiC_w on the mechanical and tribological characteristics of a hybrid composite material were investigated through various test scenarios. A Charpy pendulum was used to simulate bird strikes by inducing damage to the composites.

Incorporating 0.5 wt% of SiC_w into the hybrid laminate composite increased the UTS and energy absorption capacity of the structure by 32% and 45%, respectively. Furthermore, adding 5 wt% of self-healing agents to the structure and curing it under specific conditions increased the UTS by 4%. However, this addition also reduced the structure's energy absorption capability by 48%.

The aim of the study was to explore the effects of self-healing agents and SiC_w whiskers in hybrid composites. The results suggest that SiC_w whiskers improved the bond between the fiber and matrix, leading to enhanced UTS and energy absorption capacity. Additionally, the findings on tribological performance were promising, with the introduction of SiC_w leading to a 10% increase in wear resistance and a 20% improvement in the friction coefficient.

Overall, the research indicates that hybrid laminated composites containing both self-healing agents and SiC_w could be used in wind turbine blades to enhance their strength and energy absorption capability. The weight ratios of self-healing agents and SiC_w could be optimized in future studies based on their effects on UTS and energy absorption capacity.

ACKNOWLEDGMENTS

This research was supported by the Istanbul Technical University Office of Scientific Research Projects (ITUBAPSIS), under grant MGA-2022-43400. The authors thank to Dr. Cagatay Yilmaz for the technical discussions on the manufacturing of the self-healing capsules and M. Atif Yilmaz, Hasan Yakar, Deniz Isik and Serhat Cetin for their help during the experimental characterizations.

CONFLICT OF INTEREST STATEMENT

The authors declare that they have no known competing financial interests or personal relationships that could have appeared to influence the work reported in the article.

DATA AVAILABILITY STATEMENT

The data that support the findings of this study are available from the corresponding author upon reasonable request.

ORCID

Kemal Hasirci https://orcid.org/0009-0004-8370-515X
Berkay Ergene https://orcid.org/0000-0001-6145-1970
Alaeddin Burak Irez https://orcid.org/0000-0001-7316-7694

REFERENCES

1. Reddy SSP, Suresh R, Hanamantraygouda MB, Shivakumar BP. Use of composite materials and hybrid composites in wind turbine blades. *Mater Today Proc*. 2021;46:2827-2830. doi:10.1016/J.MATPR.2021.02.745
2. Sahoo CK, Arockiarajan A. Study of tensile-tensile fatigue behavior of patch repaired carbon-glass hybrid composite. *Polym Compos*. 2024. doi:10.1002/PC.28846
3. Kepir Y, Kara M. Influence of hydrothermal conditions on the mechanical properties of hybrid composite pipes. *J Compos Mater*. 2023;58(1):119-131. doi:10.1177/00219983231220986
4. Russel E, Nagappan B, Karsh P, et al. Effect of hygrothermal aging on novel hybrid composites: transforming textile waste into a valuable product. *Polym Compos*. 2024;45(4):3520-3535. doi:10.1002/PC.28006
5. Kong C-D, Choi S-H, Park H-B, Kim S-H. Investigation on design and impact damage for a 500W wind turbine composite blade. *Compos Res*. 2009;22(1):22-31. doi:10.7234/KSCM.2009.22.1.022
6. Ghani Olabi A, Wilberforce T, Elsaid K, et al. A review on failure modes of wind turbine components. *Energies*. 2021;14(17):1-44. doi:10.3390/en14175241
7. Kim H, Halpin JC, DeFrancisci GK. Impact Damage of Composite Structures. In: Pochiraju K, Tandon G, Schoeppner G, eds. *Long-Term Durability of Polymeric Matrix Composites*. Springer; 2012. https://doi.org/10.1007/978-1-4419-9308-3_5
8. Nanami N, Strganac T, Schneider W, Polycarpou AA. Structural and damage assessment of multi-section modular hybrid composite wind turbine blade. 2014 https://oaktrust.library.tamu.edu/handle/1969.1/153418
9. Nanami N, Ochoa OO. Damage assessment of a large-scale hybrid composite wind turbine blade. *J Mech Eng Autom*. 2016;6(5):117-127. doi:10.5923/J.JMEA.20160605.04
10. Tejas KS, Prashanth AS. Bird impact analysis of a composite wind turbine blade. *Int Res J Eng Technol*. 2017;4:637-641.
11. Verma AS, Yan J, Hu W, Jiang Z, Shi W, Teuwen JJE. A review of impact loads on composite wind turbine blades: impact threats and classification. *Renew Sustain Energy Rev*. 2023;178:113261. doi:10.1016/J.RSER.2023.113261
12. Qiu J, Chen H. Dynamic response of bird strike on variable stiffness laminates of composite leading edge. *Int J Crashworthiness*. 2022;27(2):317-327. doi:10.1080/13588265.2020.1794555
13. National Research Council. *Environmental impacts of wind-energy projects*. The National Academies Press; 2007.
14. Marris E, Fairless D. Wind farms' deadly reputation hard to shift. *Nature*. 2007;447(7141):126. doi:10.1038/447126A
15. Sovacool BK. The avian benefits of wind energy: a 2009 update. *Renew Energy*. 2013;49:19-24. doi:10.1016/J.RENENE.2012.01.074
16. Dolbeer Richard A, Wright SE. Wildlife strikes to civil aircraft in the United States, 1990–2007. 1990.
17. Long S, Mu X, Liu Y, Wang H, Zhang X, Yao X. Failure modeling of composite wing leading edge under bird strike. *Compos Struct*. 2021;255:113005. doi:10.1016/J.COMPSTRUCT.2020.113005
18. Guida M, Marulo F, Polito T, Meo M, Riccio M. Design and testing of a fiber-metal-laminate bird-strike-resistant. *Leading Edge*. 2012;46(6):2121-2129. doi:10.2514/1.43943
19. Pernas-Sánchez J, García-Rodríguez SM, Artero-Guerrero JA, López-Puente J, Costa J. High velocity impact response of carbon/epoxy composite laminates at cryogenic temperatures. *Compos Part A Appl Sci Manuf*. 2023;168:107456. doi:10.1016/J.COMPOSITESA.2023.107456
20. Zhou Y, Sun Y, Huang T. Bird-strike resistance of composite laminates with different materials. *Materials*. 2020;13(1):129. doi:10.3390/MA13010129
21. Kara M, Tatar AC, Kırıcı M, Kepir Y, Gunoz A, Avcı A. Effects of extreme low temperatures on the impact behavior of boron nitride nanofillers added carbon fiber/epoxy composite tubes. 2022;56(30):4635-4644. doi:10.1177/00219983221136278
22. Bhaskar D, Suresh G, Ganesamoorthy R, et al. Behaviour of Fibre Length in Banana Fibre Reinforced Thermoplastic Composites Under High Velocity Impact Performance. In: Palani IA, Sathiya P, Palanisamy D, eds. *Recent Advances in Materials and Modern Manufacturing: Lecture Notes in Mechanical Engineering*. Springer. 2022. https://doi.org/10.1007/978-981-19-0244-4_95
23. Jia C, Cui H, Wang Q, Li Z, Qiu Y, Yan C. Low energy impact damage characteristics of epoxy coating on the surface of sandwich composites. *Polym Compos*. 2024;45:12675-12688. doi:10.1002/PC.28659
24. Xu W, Wang Y, Gu Z, Wang P, Zhang Y, Li Y. Investigation of the static and low-velocity impact performance of 3D braided spacer composites. *Polym Compos*. 2024. doi:10.1002/PC.28853
25. Gunoz A, Kur M, Kara M. Impact response of hybrid composites under varying environmental conditions: a comparative study. *Polym Compos*. 2024;45:12481-12494. doi:10.1002/PC.28650
26. Mahesh V, Mahesh V, Harursampath D. On low velocity impact response of sandwich composite with jute/epoxy facesheet and cenosphere reinforced functionally graded core: experimental and finite element approach. *Polym Compos*. 2024;45:13151-13163. doi:10.1002/PC.28693
27. Kepir Y, Gunoz A, Kara M. Nonpenetrating repeated impact effect to the damage behavior of prestressed glass/epoxy composite pipes. *Polym Compos*. 2022;43(8):5047-5058. doi:10.1002/PC.26777
28. Donadon MV, Iannucci L, Falzon BG, Hodgkinson JM, de Almeida SFM. A progressive failure model for composite laminates subjected to low velocity impact damage. *Comput Struct*. 2008;86(11–12):1232-1252. doi:10.1016/J.COMPSTRUC.2007.11.004
29. Hayes SA, Jones FR, Marshiya K, Zhang W. A self-healing thermosetting composite material. *Compos Part A Appl Sci Manuf*. 2007;38(4):1116-1120. doi:10.1016/J.COMPOSITESA.2006.06.008
30. Yilmaz MA, Hasirci K, Yakar H, Cetin S, Isık D, Irez AB. Development of self-healing glass fiber–reinforced laminate composites for wind turbine blades. *Conf Proc Soc Exp Mech Ser*. 2024;5:33-37. doi:10.1007/978-3-031-50478-5_4
31. Simonini L, Mahmood H, Dorigato A, Pegoretti A. Evaluation of self-healing capability of a polycaprolactone interphase in epoxy/glass composites. *Compos Part A Appl Sci Manuf*. 2023;169:107539. doi:10.1016/J.COMPOSITESA.2023.107539

32. Wang Z, Li Y, Tu H. The mode II interlaminar fracture toughness and healing efficiency of repeatable self-healing composite. *Compos Part A Appl Sci Manuf*. 2022;161:107096. doi:10.1016/J.COMPOSITESA.2022.107096
33. Azevedo do Nascimento A, Fernandez FS, Ferreira E, José JD, Cysne Barbosa AP. Addition of poly (ethylene-co-methacrylic acid) (EMAA) as self-healing agent to carbon-epoxy composites. *Compos Part A Appl Sci Manuf*. 2020;137:106016. doi:10.1016/J.COMPOSITESA.2020.106016
34. Kepir Y, Gunoz A, Kara M. Repairing of damaged composite materials and self-healing composites. *Turkish J Eng*. 2022;6(2):149-155. doi:10.31127/TUJE.866955
35. Hayes SA, Zhang W, Branthwaite M, Jones FR. Self-healing of damage in fibre-reinforced polymer-matrix composites. *J R Soc Interface*. 2007;4(13):381-387. doi:10.1098/RSIF.2006.0209
36. Kessler MR, Sottos NR, White SR. Self-healing structural composite materials. *Compos Part A Appl Sci Manuf*. 2003;34(8):743-753. doi:10.1016/S1359-835X(03)00138-6
37. Lee JW, Gangadharan SN, Mirmirani M, Raffa A. Multidisciplinary design optimization of a hybrid composite wind turbine blade. *ASME 2011 Int Manuf Sci Eng Conf*. 2011;2:79-88. doi:10.1115/MSEC2011-50204
38. Pheysey J, De Cola F, Martinez-Hergueta F. Short fibre/unidirectional hybrid thermoplastic composites: experimental characterisation and digital analysis. *Compos Part A Appl Sci Manuf*. 2024;181:108121. doi:10.1016/J.COMPOSITESA.2024.108121
39. Wang H, Zhu K, Tang Z, Zhou Y, Pan D. Investigation of tribological behavior of polytetrafluoroethylene/graphene composite. *Polym Compos*. 2024;45(16):15293-15306. doi:10.1002/PC.28838
40. Vezhavendhan R, Ganesamoorthy R, Suresh G, et al. A tribological investigation of fly ash particulate-loaded E-glass fiber reinforced interpenetrating polymer network composites. *Polym Compos*. 2024;45:13348-13358. doi:10.1002/PC.28707
41. Suresh G, Rajasekharan V, Vijayendra Gopal K, et al. Analyzing the tribological behavior of titanium dioxide (TiO2) particulate filled jute fiber reinforced interpenetrating polymer network (IPNs) composite by using Taguchi optimization technique. *Tribology Ind*. 2023;45(2):226-236. doi:10.24874/ti.1448.02.23.04
42. Gopal KV, Kumar KRV, Suresh G, Rajasekharan V, Nagarajan PK, Meenakshi CM. Investigation of TiO_2 nano filler in mechanical, thermal behaviour of sisal/jute fiber reinforced interpenetrating polymer network (IPN) composites. *Mater Res*. 2022;25:e20220406. doi:10.1590/1980-5373-MR-2022-0406
43. Jeevamalar J, Abbas SM, Kumar SB, et al. *Influence of nanoclay dispersion on mechanical and vibration properties of E-glass fiber-reinforced IPN composites*. Springer; 2022 https://link.springer.com/chapter/10.1007/978-981-19-0244-4_25
44. Shinoda Y, Yoshida M, Akatsu T, Wakai F. Effect of amount of boron doping on compression deformation of fine-grained silicon carbide at elevated temperature. *J Am Ceram Soc*. 2004;87(8):1525-1529. doi:10.1111/J.1551-2916.2004.01525.X
45. Yamamoto T, Kitaura H, Kodera Y, Ishii T, Ohyanagi M, Munir ZA. Consolidation of nanostructured β-SiC by spark plasma sintering. *J Am Ceram Soc*. 2004;87(8):1436-1441. doi:10.1111/J.1551-2916.2004.01436.X
46. Vaßen R, Kaiser A, Förster J, Buchkremer HP, Stöver D. Densification of ultrafine SiC powders. *J Mater Sci*. 1996;31(14):3623-3637. doi:10.1007/BF00352770/METRICS
47. Kara M, Erdag Nomer A, Kepir Y, Gunoz A, Avci A. Low-energy repeated impact response of nanoparticle reinforced carbon fiber epoxy composite pipes. *Compos Struct*. 2022;299:116100. doi:10.1016/J.COMPSTRUCT.2022.116100
48. Maître A, Vande PA, Laval JP, Valette S, Trolliard G. Role of boron on the spark plasma sintering of an α-SiC powder. *J Eur Ceram Soc*. 2008;28(9):1881-1890. doi:10.1016/J.JEURCERAMSOC.2008.01.002
49. Zhou Y, Hirao K, Toriyama M, Tanaka H. Very rapid densification of nanometer silicon carbide powder by pulse electric current sintering. *J Am Ceram Soc*. 2000;83(3):654-656. doi:10.1111/J.1151-2916.2000.TB01249.X
50. Abdelal NR, Aljarrah MT. The effect of silicon carbide whiskers on the mode I interlaminar fracture of carbon fiber composites. *Ceram Int*. 2018;44(3):2700-2708. doi:10.1016/J.CERAMINT.2017.10.220
51. Qian M, Xu X, Qin Z, Yan S. Silicon carbide whiskers enhance mechanical and anti-wear properties of PA6 towards potential applications in aerospace and automobile fields. *Compos Part B Eng*. 2019;175:107096. doi:10.1016/J.COMPOSITESB.2019.107096
52. Ahmad B, Fang X. Modeling shear behavior of woven fabric thermoplastic composites for crash simulations. *Appl Compos Mater*. 2020;27(6):739-765. doi:10.1007/S10443-020-09844-0/TABLES/4
53. Ekşi S, Genel K. Comparison of mechanical properties of unidirectional and woven carbon, glass and aramid fiber reinforced epoxy composites. *Phys Pol A*. 2017. https://bibliotekanauki.pl/articles/1031946.pdf;132:879-882.
54. Bert CW. Classical Lamination Theory. In: Pendleton RL, Tuttle ME, eds. *Manual on Experimental Methods for Mechanical Testing of Composites*. Springer. 1989. https://doi.org/10.1007/978-94-009-1129-1_3
55. Blaiszik BJ, Caruso MM, McIlroy DA, Moore JS, White SR, Sottos NR. Microcapsules filled with reactive solutions for self-healing materials. *Polymer*. 2009;50(4):990-997.
56. ASTM International. Standard test method for tensile properties of polymer matrix composite materials 1. 2014 10.1520/D3039_D3039M-1
57. Systemes D. *Getting started with abaqus: interactive edition abaqus 6.8*. Dassault Systemes; 2008.
58. Lapczyk I, Hurtado JA. Progressive damage modeling in fiber-reinforced materials. *Compos Part A Appl Sci Manuf*. 2007;38(11):2333-2341. doi:10.1016/J.COMPOSITESA.2007.01.017
59. Iannucci L, Willows ML. An energy based damage mechanics approach to modelling impact onto woven composite materials—part I: numerical models. *Compos Part A Appl Sci Manuf*. 2006;37(11):2041-2056. doi:10.1016/J.COMPOSITESA.2005.12.013
60. Iannucci L, Donadon MV. Bird strike modeling using a new woven glass failure model. 4:18-41. https://www.researchgate.net/publication/267788157
61. Iannucci L. Progressive failure modelling of woven carbon composite under impact. *Int J Impact Eng*. 2006;32(6):1013-1043. doi:10.1016/J.IJIMPENG.2004.08.006
62. Strugala G, Landowski M, Zaremba M, Turowski J, Szkodo M. Impact resistance of plain and twill fabric in GFRP measured by active thermography. *Adv Compos Lett*. 2018;27(5):176-184. doi:10.1177/096369351802700501/ASSET/IMAGES/LARGE/10.1177_096369351802700501-FIG8.JPEG

63. Muralidhara B, Kumaresh Babu SP, Suresha B. Utilizing vacuum bagging process to prepare carbon fiber/epoxy composites with improved mechanical properties. *Mater Today Proc*. 2020; 27:2022-2028. doi:10.1016/J.MATPR.2019.09.051
64. ASTM International. D6110 standard test method for determining the Charpy impact resistance of notched specimens of plastics. 2018 https://www.astm.org/d6110-18.html
65. Doeland W. EASA CM-S-001-compliance with CS-25 bird strike requirements. 2012 https://www.easa.europa.eu/en/document-library/product-certification-consultations/easa-cm-s-001
66. Zhou Y, Pervin F, Jeelani S, Mallick PK. Improvement in mechanical properties of carbon fabric–epoxy composite using carbon nanofibers. *J Mater Process Technol*. 2008;198(1–3):445-453. doi:10.1016/J.JMATPROTEC.2007.07.028
67. Jonathan SM, Kumar SL, Kumar SM, Nayak SS. Effect of silicon carbide fillers on the mechanical properties of glass fibre reinforced epoxy polymer composite. *Int Res J Eng Technol*. 2021;8(7):4032-4036. www.irjet.net
68. Palle RR, Schuster J, Shaik YP, et al. Fabrication and characterization of glass fiber with SiC reinforced polymer composites. *Open J Compos Mater*. 2021;12(1):16-29. doi:10.4236/OJCM.2022.121002
69. Abot JL, Song Y, Schulz MJ, Shanov VN. Novel carbon nanotube array-reinforced laminated composite materials with higher interlaminar elastic properties. *Compos Sci Technol*. 2008;68(13): 2755-2760. doi:10.1016/J.COMPSCITECH.2008.05.023
70. Suriani MJ, Rapi HZ, Ilyas RA, Petrů M, Sapuan SM. Delamination and manufacturing defects in natural fiber-reinforced hybrid composite: a review. *Polymer*. 2021;13(8):1323. doi:10.3390/POLYM13081323
71. Imran M, Khan R. A review on the effect of delamination on the performance of composite plate. *J Sci Ind Res Ser A Phys Sci*. 2018;61:173-182.
72. Hwang SF, Mao CP. Failure of delaminated interply hybrid composite plates under compression. *Compos Sci Technol*. 2001;61(11):1513-1527. doi:10.1016/S0266-3538(01)00048-3
73. Zhang B, Kawashita LF, Jones MI, Lander JK, Hallett SR. An experimental and numerical investigation into damage mechanisms in tapered laminates under tensile loading. *Compos Part A Appl Sci Manuf*. 2020;133:105862. doi:10.1016/J.COMPOSITESA.2020.105862
74. Tasdemir B, Coker D. Comparison of damage mechanisms in curved composite laminates under static and fatigue loading. *Compos Struct*. 2019;213:190-203.
75. Ergene B, Bolat C, Karakilinc U, Irez AB. A comprehensive investigation of drilling performance of anisotropic stacked glass-carbon fiber reinforced hybrid laminate composites. *Polym Compos*. 2023;44(5):2656-2670. doi:10.1002/PC.27268
76. Celik E, Sacmaozu G, Irez AB. Development of carbon-glass fiber reinforced hybrid composites: applications in offshore wind turbine blades. *Conf Proc Soc Exp Mech Ser*. 2022;3:17-22. doi:10.1007/978-3-030-86741-6_4
77. Irez AB. Biaxial fatigue failure of short glass fiber reinforced polyamide 6,6: an in-depth investigation of stiffness drop and microstructural evolution. *J Thermoplast Compos Mater*. 2024; 2:3294-3318.
78. ASTM International. ASTM G99-17-standard test method for wear testing with a pin-on-disk apparatus. 2023 https://webstore.ansi.org/standards/astm/astmg9917
79. Antil P, Singh S, Manna A. SiC p/glass fibers reinforced epoxy composites: wear and erosion behavior. *Indian J Eng Mater Sci*. 2018;25:122-130.
80. Irez AB, Miskioglu I, Bayraktar E. *Mechanical characterization of epoxy–scrap rubber based composites reinforced with nano graphene. Mechanics of Composite and Multi-Functional Materials, Volume 6: Proceedings of the 2017 Annual Conference on Experimental and Applied Mechanics*. Springer International Publishing; 2018:45-57.
81. Mohan N, Mahesha CR, Raja R. Tribo-mechanical behaviour of SiC filled glass-epoxy composites at elevated temperatures. *Int J Eng Sci Technol*. 2014;6(5):44-56. doi:10.4314/IJEST.V6I5.5
82. Fouquet S, Rollin M, Pailler R, Bourrat X. Tribological behaviour of composites made of carbon fibres and ceramic matrix in the Si–C system. *Wear*. 2008;264(9–10):850-856. doi:10.1016/J.WEAR.2006.12.081
83. Power AC. Decommissioned wind turbine blade management strategies. American Clean Power Association. 2023 https://etipwind.eu/files/reports/
84. Boltman S. Offshore wind: opportunities for the composites industry. 2011.

SUPPORTING INFORMATION

Additional supporting information can be found online in the Supporting Information section at the end of this article.

How to cite this article: Hasirci K, Ergene B, Irez AB. Tribologically enhanced self-healing hybrid laminates for wind turbine applications. *Polym Compos*. 2024;1-19. doi:10.1002/pc.29247